Dense/Porous Asymmetric-Structured Oxygen Permeable Membranes Based on $La_{0.6}Ca_{0.4}CoO_3$ Perovskite-Type Oxide

Ken Watanabe,[†] Masayoshi Yuasa,[‡] Tetsuya Kida,[‡] Kengo Shimanoe,*[,‡] Yasutake Teraoka,[‡] and Noboru Yamazoe[‡]

Department of Molecular and Material Sciences, Interdisciplinary Graduate School of Engineering Science, and Department of Material Sciences, Faculty of Engineering Sciences, Kyushu University, Kasuga-Koen 6-1, Kasuga-shi, Fukuoka 816-8580, Japan

Received May 20, 2008. Revised Manuscript Received September 12, 2008

To achieve high-efficiency oxygen permeation using mixed (ionic and electronic) conducting perovskite-type oxides, we examined asymmetric-structured membranes of $La_{0.6}Ca_{0.4}CoO_3$ in which a thin dense membrane was deposited on a porous support. The $La_{0.6}Ca_{0.4}CoO_3$ porous support was fabricated using irregular-shaped precursor particles prepared through an oxalate method. The fabricated support had good gas permeability and thermal stability, showing sufficient properties as a support for dense thin membranes. A dense membrane of 10 μm thickness was successfully formed on the porous support by coating a $La_{0.6}Ca_{0.4}CoO_3$ slurry and subsequent densification by sintering. The deposited thin membrane was gastight and free from clacks, as revealed by gas permeation tests and SEM observations. The asymmetric membrane exhibited a high oxygen permeability of 1.66 cm^3 (STP, standard temperature and pressure) min^{-1} cm^{-2} at 930 °C, which was four times higher than that of a typical sintered-disk type membrane with 1200 μm thickness, demonstrating its feasibility as a high-performance oxygen separation membrane.

Introduction

Mixed oxide ionic and electronic conductors have a promising possibility as oxygen permeable membranes without electrodes and external circuitry at elevated temperatures. If such ceramic membranes with high oxygen permeability are developed, clean and efficient membrane processes would become available for industrial oxygen separation utilizing waste heat. Since Teraoka et.al. first reported an oxygen separation process using mixed conductor membranes derived from cobalt-based perovskite-type oxides in 1985,[1] many kinds of perovskite-type oxides have been developed for oxygen permeable membranes.[2−16] Among them, membranes based on $SrCo_{0.8}Fe_{0.2}O_{3-\delta}$,[1] $Ba_{0.5}Sr_{0.5}Co_{0.8}Fe_{0.2}O_{3-\delta}$,[3] $SrCo_{0.9}Nb_{0.1}O_{3-\delta}$,[16] and $SrCo_{0.95}Sc_{0.05}O_{3-\delta}$[17] showed high oxygen permeabilities. However, the oxygen permeation rate of these membranes still ranges from 2 to 4 cm^3 min^{-1} cm^{-2}, not sufficiently high for a practical use; an oxygen permeation flux of more than 10 cm^3 min^{-1} cm^{-2} is required with respect to efficiency and costs.[18] Therefore, a remarkable improvement in the oxygen permeation rate is strongly demanded. It is well-known that oxygen permeation properties of perovskite membranes are dependent on composition, partial or total substitution of A or B site cation for another cation,[1−17] membrane thickness,[19−21] and surface morphology.[22−25] Hence, careful control of these parameters is crucial to achieve high oxygen permeation.

* Corresponding author. E-mail: simanoe@mm.kyushu-u.ac.jp. Fax: 81-92-583-7538. Tel: 81-92-583-7539.
[†] Department of Molecular and Material Sciences, Kyushu University.
[‡] Department of Material Sciences, Kyushu University.

(1) Teraoaka, Y.; Zhang, H. M.; Furukawa, S.; Yamazoe, N. *Chem. Lett.* **1985**, 1743–1746.
(2) Teraoka, Y.; Nobunaga, T.; Yamazoe, N. *Chem. Lett.* **1988**, 503–506.
(3) Shao, Z.; Xiong, G.; Tong, J.; Dong, H.; Yang, W. *Sep. Purif. Technol.* **2001**, 419–429.
(4) Shao, Z.; Yang, W.; Cong, Y.; Dong, H.; Tong, J.; Xiong, G. *J. Membr. Sci.* **2000**, *172*, 177–186.
(5) Ishihara, T.; Yamada, T.; Arikawa, H.; Nishiguchi, H.; Takita, Y. *Solid State Ionics* **2000**, *135*, 631–636.
(6) Elshof, J. E. T.; Bouwmeester, H. J. M.; Verweij, H. *Solid State Ionics* **1995**, *81*, 97–109.
(7) Zhu, X.; Wang, H.; Yang, W. *Chem. Commun.* **2004**, 1130–1131.
(8) Miura, N.; Murae, H.; Kusaba, H.; Tamaki, J.; Sakai, G.; Yamazoe, N. *J. Electrochem. Soc.* **1999**, *146*, 2581–2586.
(9) Kusaba, H.; Sakai, G.; Miura, N.; Yamazoe, N. *Electrochemistry* **2000**, *68*, 409–411.
(10) Kharton, V. V.; Viskup, A. P.; Kovalevsky, A. V.; Figueiredo, F. M.; Jurado, J. R.; Yaremchenko, A.-A.; Naumovich, E.-N.; Frade, J. R. *J. Mater. Chem.* **2000**, *10*, 1161–1169.
(11) Kharton, V. V.; Kovalevsky, A. V.; Viskup, A. P.; Jurado, J. R.; Figueiredo, F. M.; Naumovich, E. N.; Frade, E. N. *J. Solid State Chem.* **2001**, *156*, 437–444.
(12) Kinoshita, K.; Kusaba, H.; Sakai, G.; Shimanoe, K.; Miura, N.; Yamazoe, N. *Chem. Lett.* **2001**, 344–345.
(13) Wang, H; Tablet, C.; Feldhoff, A.; Caro, J. *Adv. Mater.* **2005**, *17*, 1785–1788.
(14) Teraoka, Y.; Shimokawa, T.; Kang, C. Y.; Kusaba, H.; Sasaki, K. *Solid State Ionics* **2006**, *177*, 2245–2248.
(15) Dong, X.; Xu, Z.; Chang, X.; Zhang, C.; Jin, W. *J. Am. Ceram. Soc.* **2007**, *90*, 3923–3929.
(16) Nagai, T.; Itoh, W.; Sakon, T. *Solid State Ionics* **2007**, *177*, 3433–3444.
(17) Zeng, P.; Ran, R.; Chen, Z.; Gu, H.; Shao, Z. *AIChE J.* **2007**, *53*, 3116–3124.
(18) *Technical Report for Development of Hydrogen-Manufacturing Technology from Steel-Making By-Product Gases*; The Japan Research and Development Center for Metals Foundation: Tokyo, 2006.
(19) Chen, C. H.; Bouwmeester, H. J. M.; Doorn, R. H. E.; Kruidhof, H.; Burggraaf, A. J. *Solid State Ionics* **1997**, *98*, 7–13.
(20) Haung, K.; Goodenough, J. B. *J. Electrochem. Soc.* **2001**, *148*, E203–E214.
(21) Chen, C.; Zhang, Z.; Jiang, G.; Fan, C.; Liu, W.; Bouwmeester, H. J. M. *Chem. Mater.* **2001**, *13*, 2797–2800.
(22) Kharton, V. V.; Kovalevsky, A. V.; Yaremchenko, A. A.; Figueiredo, F. M.; Naumovich, E. N.; Shaulo, A. L.; Marques, F. M. B. *J. Membr. Sci.* **2002**, *195*, 277–287.
(23) Teraoka, Y.; Honbe, Y.; Ishii, J.; Furukawa, H.; Moriguchi, I. *Solid State Ionics* **2002**, *152−153*, 681–687.

10.1021/cm8013144 CCC: $40.75
Published on Web 10/29/2008

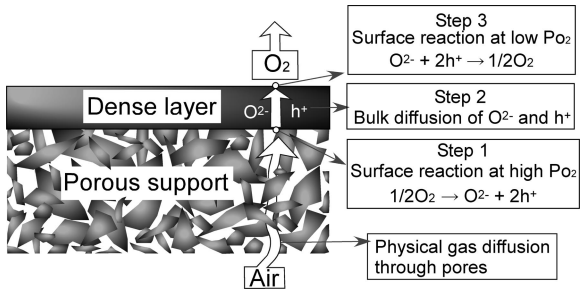

Figure 1. Schematic model of a dense/porous asymmetric-structured membrane.

Oxygen permeation through a mixed oxide conductor membrane is believed to take place through three steps as follows: (step 1) oxygen adsorption and dissociation into oxide ions at the high oxygen partial pressure side (cathode side) of the membrane surface, (step 2) oxide-ion diffusion through the bulk of the membrane, (step 3) release of oxide ions into molecular oxygen and oxygen desorption at the low oxygen partial pressure side (anode side) of the membrane surface. Accordingly, if the oxygen permeation in mixed oxide conductors is governed only by bulk diffusion of oxide ions (step 2), the oxygen permeation rate would increase with decreasing the membrane thickness because of a decrease in the diffusion length of oxide ion. Indeed, it has been reported that the oxygen permeability of a $La_{0.6}Sr_{0.4}Co_{0.8}Fe_{0.2}O_3$ membrane increased with decreasing the thickness from 1.3 mm to 200 μm, reaching a high oxygen permeability of 3.8 $cm^3\ min^{-1}\ cm^{-2}$.[26] Therefore, it is readily expected that reducing the membrane thickness from millimeter to micrometer sizes such as 1−10 μm would remarkably improve the oxygen permeation efficiency. However, there is a problem of lack of mechanical strength in such thin self-standing membranes.

To solve this problem, we have devised an asymmetric-structured membrane, i.e., a thin dense membrane deposited on a porous support, as shown in Figure 1. Teraoka et al. were the first to successfully fabricate a $La_{0.6}Sr_{0.4}CoO_3$ (LSC) asymmetric membrane, for which the thickness of the dense layer was about 15 μm, demonstrating the feasibility of this concept for improving the oxygen permeability.[27,28] The porous support was fabricated by packing large aggregated particles (more than 10 μm in diameter) calcined at 1400 °C into a disk and subsequent sintering at 1400 °C. The dense layer was formed on the support by a splay deposition technique using a LSC suspension and sintered at 1400 °C. However, the oxygen permeability of the asymmetric membrane was lower than that expected because of the following reasons; (1) the chemical composition at the surface of the dense layer was different from that of the bulk due to sintering at high temperature (1400 °C), (2) the effective area for oxygen permeation was low because of large pore sizes (10−50 μm) and the resulting poor distribution of pores in the support. From these results, it appears that lowering fabrication temperature and controlling the pore size in the support are important to achieve high oxygen permeation.

Other researchers have also reported the fabrication and properties of asymmetric-structured membranes,[29−38] tubes[39] and fiber.[40] In particular, Ito et al. have fabricated a $SrCo_{0.9}Nb_{0.1}O_3$-based asymmetric-structured tube in which a thin layer of about 50 μm thickness was deposited on a porous tube, and they succeeded in separating oxygen from a compressed air (1.0 MPa) at a high permeation rate of 9 $cm^3\ min^{-1}\ cm^{-2}$ at 900 °C.[37] In addition, Wang et al. reported that $BaCo_xFe_yZr_zO_3$-based fiber, which consisted of dense layer at the outer surface and porous layer in the middle of fiber, showed high oxygen permeability (7.5 $cm^3\ min^{-1}\ cm^{-2}$ at 900 °C).[40] These studies clearly showed the promising features of asymmetric-structured membranes for high-performance oxygen separation, although both results cannot be compared simply because their operation conditions are different. However, the fabrication of asymmetric membranes is still a challenge because of difficulty in obtaining porous supports with desirable properties in terms of pore size, gas permeability, and thermal stability. Frequently, pore-forming agents such as cellulose, starch, polymer, and carbon are used for the fabrication of porous supports.[27,30−32,34−39] High-temperature combustion of these organic agents mixed with perovskite-type oxides leads to the formation of pores in the supports. However, this method often produces closed pores rather than open pores that are connected to the surface, and the resulting pore sizes are large and inhomogeneous. Thus, a new fabrication method is required to control the size and morphology of pores in porous supports.

Recently, we have reported the oxygen permeation properties of a $La_{0.6}Ca_{0.4}CoO_3$ asymmetric-structured membrane fitted with an oxygen evolution (catalyst) layer in a short paper.[41] $La_{0.6}Ca_{0.4}CoO_3$ has a good sinterability, meaning that it is possible to make dense/porous asymmetric-structured membrane. Therefore $La_{0.6}Ca_{0.4}CoO_3$ was chosen as a membrane material. The fabricated asymmetric membrane

(24) Lee, S.; Lee, K.-S.; Woo, S.-K.; Kim, J.-W.; Ishihara, T.; Kim, D.-K. *Solid State Ionics* **2003**, *158*, 287–296.
(25) Kusaba, H.; Shibata, Y.; Sasaki, K.; Teraoka, Y. *Solid State Ionics* **2006**, *177*, 2249–2253.
(26) Miura, N.; Okamoto, Y.; Tamaki, J.; Morinaga, K.; Yamazoe, N. *Solid State Ionics* **1995**, *79*, 195–200.
(27) Teraoaka, Y.; Fukuda, T.; Miura, N.; Yamazoe, N. *J. Ceram. Soc. Jpn., Int. Ed.* **1989**, *97*, 523–529.
(28) Teraoaka, Y.; Fukuda, T.; Miura, N.; Yamazoe, N. *J. Ceram. Soc. Jpn., Int. Ed.* **1989**, *97*, 533–538.
(29) Haar, L. M. V. D.; Verweij, H. *J. Memb, Sci.* **2000**, *180*, 147–155.
(30) Jin, W.; Li, S.; Haung, P.; Xu, N.; Shi, J. *J. Membr. Sci.* **2001**, *185*, 237–243.
(31) Vente, J.-F.; Haije, W.-G.; Rak, Z.-S. *J. Membr. Sci.* **2006**, *276*, 178–184.
(32) Ikeguchi, M.; Ishii, K.; Sekine, Y.; Kikuchi, E.; Matsukata, M. *Mater. Lett.* **2005**, 1356–1360.
(33) Chang, X.; Zhang, C.; Jin, W.; Xu, N. *J. Membr. Sci.* **2006**, *285*, 232–238.
(34) Kovalevsky, A. V.; Kharton, V. V.; Snijkers, F. M. M.; Cooymans, J. F. C.; Luyten, J. J.; Marques, F. M. B. *J. Membr. Sci.* **2007**, *301*, 238–244.
(35) Araki, S.; Hoshi, Y.; Hamakawa, S.; Hikazudani, S.; Mizukami, F. *Solid State Ionics* **2008**, *178*, 1740–1745.
(36) Kovalevsky, A. V.; Kharton, V. V.; Maxim, F.; Shaula, A. L.; Frade, J R. *J. Membr. Sci.* **2006**, *278*, 162–172.
(37) Itoh, W.; Nagai, T.; Sakon, T. *Solid State Ionics* **2007**, *178*, 809–816.
(38) Etchegoyen, G.; Chartier, T.; Gallo, P.-D. *J. Eur. Ceram. Soc.* **2006**, *26*, 2807–1815.
(39) Yin, X.; Hong, L.; Liu, Z. L. *J. Membr. Sci.* **2006**, *268*, 2–12.
(40) Wang, H.; Schiestel, T.; Tablet, C.; Schroeder, M.; Caro, J. *Solid State Ionics* **2006**, *177*, 2255–2259.
(41) Watanabe, K.; Yuasa, M.; Kida, T.; Shimanoe, K.; Teraoaka, Y.; Yamazoe, N. *Solid State Ionics* **2008**, *179*, 1377–1381.

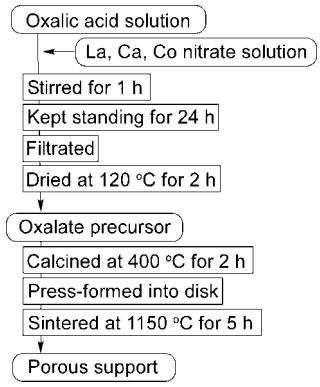

Figure 2. Fabrication process of porous supports by an oxalate method.

achieved a high oxygen permeation flux of 4.8 $cm^3\ min^{-1}\ cm^{-2}$ from air (normal pressure) at 930 °C. In this present paper, we mainly focus on the fabrication of the $La_{0.6}Ca_{0.4}CoO_3$-asymmetric-structured membrane. For the fabrication of supports, the following criteria were raised at the beginning of the study: (1) The gas permeability should be more than $6 \times 10^{-4}\ cm^3cm.min^{-1}Pa^{1-}cm^{-2}$, which is high enough not to limit oxygen supply and to attain a desired oxygen permeation flux of more than 10 $cm^3\ min^{-1}\ cm^{-2}$. (2) The size of pores in the supports should be 1−3 μm to deposit a membrane in the range of 10−50 μm thick. To meet the above criteria, porous supports were fabricated by an oxalate method that can produce perovskite precursor particles with a low sinterability. Here, we report the fabrication detail of the $La_{0.6}Ca_{0.4}CoO_3$ dense/porous asymmetric membrane, that is, the effects of fabrication conditions on the properties of porous supports such as composition, crystal structure, pore size distribution, gas permeability, and thermal stability. The structure of the asymmetric membrane and its oxygen permeability are also discussed.

Experimental Section

(a) Fabrication of Asymmetric Membranes. *(i) Fabrication of Porous Supports.* LCC ($La_{0.6}Ca_{0.4}CoO_3$) porous supports were fabricated by an oxalate method, as follows. The fabrication procedure is shown in Figure 2. Lanthanum, calcium, and cobalt nitrates in a designated molar ratio were dissolved in 80 mL of deionized water, and then the mixed nitrate solution was dropped through a burette into 100 mL of an oxalic acid solution (0.9 mol/L) at 30 °C under stirring. The resulting pink-colored suspension thus obtained was further stirred for 1 h, kept standing for 24 h, and filtrated to collect the solid precursor. The precursor powder was dried at 120 °C for 2 h, and then calcined at 400 °C for 2 h. The calcined powder was press-formed into discs of 20 mm and 2 mm in diameter and thickness, respectively, which were then sintered at 1100−1175 °C in air for 5 h.

(ii) Fabrication of Dense Layers on the Porous Supports. Dense LCC layers were formed on the porous supports by a simple slurry-coating method. LCC powder for coating was prepared through an amorphous malic-acid precursor (AMP) method using malic acid as a complexing agent.[42] Lanthanum, calcium and cobalt nitrates were dissolved in 50 mL of deionized water, and the resulting solution was mixed with 50 mL of a malic acid solution. The molar ratio of malic acid to total metal ions was set to 1.5. The pH of the mixed aqueous solution was adjusted to 3 with aqueous ammonia (28%). The mixed solution was evaporated to dryness, and then calcined in air at 900 °C. The calcinated powder was grounded and dispersed in ethanol to obtain a slurry for coating (1−20 wt %). Three-tenths of a milliliter of slurry containing the prepared LCC powder was dropped on the porous supports to form LCC layers, which was then dried at room temperature for 1 day and finally sintered at 1150 °C for 5 h.

(b) Characterization. The crystal structure of the perovskite-type oxide was characterized by powder X-ray diffraction (XRD) with Cu Kα radiation (RINT2100, Rigaku Co., Ltd.). Elemental analysis of the porous supports was carried out by X-ray fluorescence analysis (XRF) (ZXmini, Rigaku Co., Ltd.). The morphologies of the porous supports and the asymmetric membrane were observed on a scanning electron microscope (JSM-6340F, JEOL Co., Ltd.). The porosity and gas permeability of the porous supports were evaluated by mercury porosimetry and by measuring their nitrogen permeation rates, respectively. The nitrogen permeation rates were determined by an airtight measurement at room temperature. For the measurement, a differential pressure was applied across the membrane while the pressure of the low-pressure side of porous support was kept atmospheric pressure. The nitrogen permeation rates were measured with a mass flow meter.

(c) Oxygen Permeation Measurements. The oxygen permeability through the asymmetric membrane was measured with the same apparatus as used in previous studies.[9] A dense layer side of the asymmetric membrane was fixed with a quartz tube using a silver ring as an adhesive agent at 960−965 °C. Oxygen permeation measurements were performed by supplying CO_2-less synthetic air (200 $cm^3\ min^{-1}$) and He sweep gas (120 $cm^3\ min^{-1}$) to porous support and dense layer, respectively, at 630−930 °C. The concentration of permeated oxygen was analyzed by a Thermal Conductivity Detector (TCD) gas chromatograph directly connected to the effluent line of dense layer side.

Results and Discussion

Optimization of Processing Conditions and Characterization of the Porous Supports. For the fabrication of porous supports, it is considered that a starting powder with a low sinterability is useful because particles with an anisotropic shape such as rod, disk, and wire are difficult to be sintered rather than spherical particles. As an extensive search for a method possible to produce anisotropic-shaped particles, we found that the use of oxalic acid as both precipitatin- and complexing agents finally gives rodlike particles in micrometer size. On the basis of these findings, we tried to fabricate porous LCC supports stable at higher temperatures by the oxalate method.

First, the crystal structure and composition of the fabricated supports were analyzed by XRD and XRF, respectively. Patterns a and b in Figure 3 show the XRD patterns of porous supports sintered at 1150 °C for 5 h. When precursor particles were prepared in the stoichiometric ratio, the pattern of the support was ascribed to the rhombohedral perovskite phase[43] with low oxygen permeability, as shown in Figure 3a. The deviation from the stoichiometric composition was confirmed by XRF, as shown in Table 1 (run 1), which shows that Ca/La and Co/La ratios were smaller than the stoichiometric

(42) Teraoka, Y.; Kakebayashi, H.; Moriguchi, I.; Kagawa, S. *Chem. Lett.* **1991**, 673–676.

(43) Ohno, Y.; Nagata, S.; Sato, H. *Solid State Ionics* **1983**, *9−10*, 1001–1008.

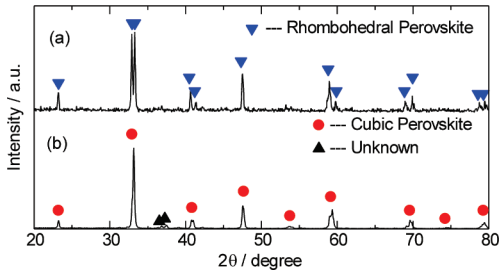

Figure 3. XRD patterns of porous supports fabricated by the oxalate method (a) without and (b) with the control of starting metal nitrate ratios.

Table 1. Elemental Analysis Results of Porous Supports by X-ray Fluorescence Measurements

run	starting ratio (mol) La:Ca:Co	measured ratio (mol) La:Ca:Co
1 (stoichiometric)	6:4:10	6:0.2:7.5
2	6:6:10	6:4:8.6
3	6:8:12	6:5:8.7
4	6:6:12	6:3.8:10.9
5	6:8:12	6:5:10

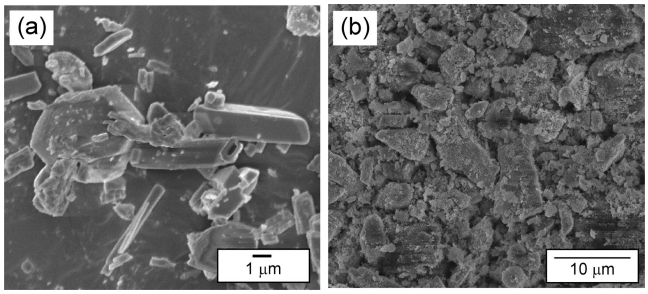

Figure 4. SEM photographs of (a) as-prepared precursor particles by the oxalate method (dried at 120 °C) and (b) the surface of the green support packed with the LCC ($La_{0.6}Ca_{0.4}CoO_3$) particles calcined at 400 °C.

ratios. Because this method is based on the precipitation and complexation of metal oxalates, the observed deviation from the stoichiometric composition is considered to be due to slower precipitation rates of Co and Ca oxalates or their higher solubility in water than that of La oxalate. The above results indicate that the processing conditions of the oxalate method need to be optimized to achieve the desired stoichiometry. Generally, the precipitation rates of metal oxalates are strongly affected by concentration of oxalic acid, ratio of metal cations to oxalic acid, and temperature. Therefore, theses parameters should be controlled carefully. As a result of delicate variations in the parameters, we successfully obtained a $La_{0.6}Ca_{0.4}CoO_3$ porous support with near the stoichiometric composition when the molar ratio of La:Ca:Co was 1:1:2 at 30 °C, as shown in Table 1 (run 4). Figure 3b shows the XRD patterns of a porous support prepared with the optimized conditions. The crystal phase of the porous support was found to be the cubic perovskite-type,[43] suggesting successful control of the material stoichiometry by optimizing the oxalate method, although an impurity (unknown) phase was slightly seen in the XRD pattern. The very small impurity phase seems to be caused by a little deviation from stoichiometric composition.

Figure 4a shows the SEM image of precursor particles prepared through the oxalate method. It clearly shows that the as-prepared oxalate precursor particles are of irregular

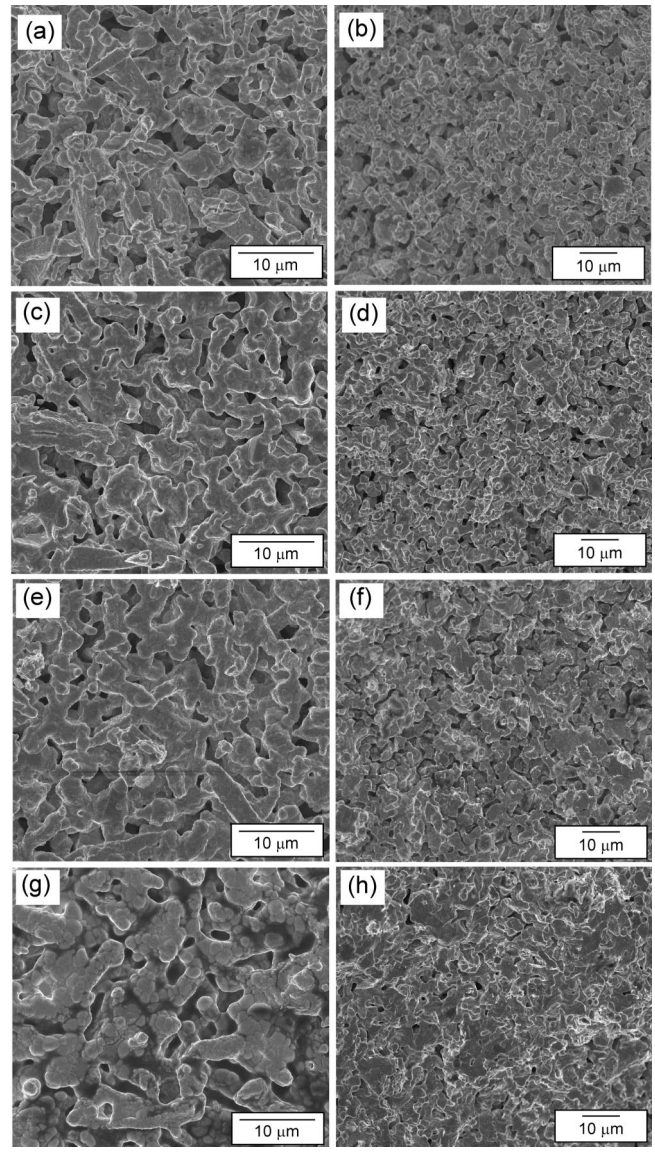

Figure 5. SEM photographs of the surface of the porous supports sintered at (a) 1100, (c) 1125, (e) 1150, and (g) 1175 °C, together with cross-sectional views for (b) 1100, (d) 1125, (g) 1150, and (h) 1175 °C.

shape with a wide size distribution. Figure 4b shows the surface SEM images of a green support composed of the precursor particles calcined at 400 °C. Many large pores ranging from 1 to 5 μm were observed in the green support because of a low packing density of the irregular- and anisotropic-shaped particles. Figure 5 shows the SEM images of the surface and cross section of the porous supports prepared through the optimized method with different sintering temperatures from 1100 to 1175 °C. It is obvious that the openings resulted from low packing densities of the irregular-shaped particles were remained even after treatments at high temperature, although the particles are sintered to a certain extent. This observation shows the effectiveness of the present approach to fabricate porous supports. The SEM micrographs indicate that the size of open pores was estimated to be around 1−2 μm. This value is desirable as a pores size of porous supports in terms of gas permeation rate, mechanical strength, and deposition of dense films composed of 1−3 μm sized particles. A further increase in the pore size, i.e., larger than 50 μm, may reduce the

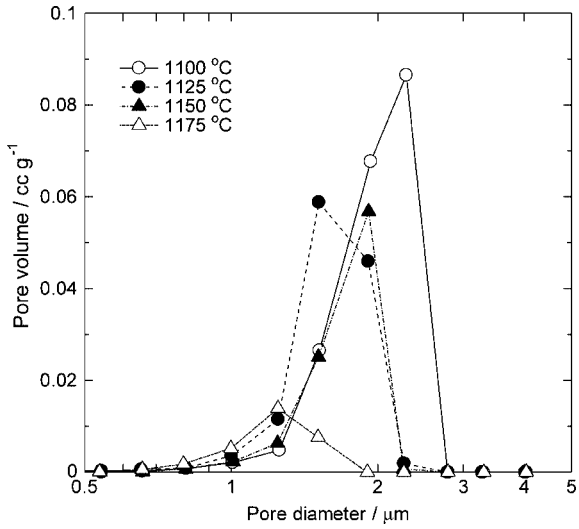

Figure 6. Pore size distribution for the porous supports sintered at different temperatures of 1100−1175 °C.

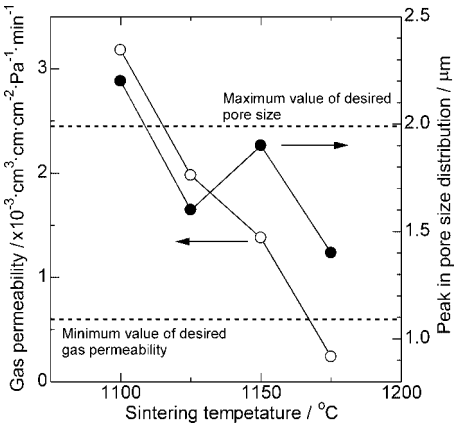

Figure 7. Dependence of the gas permeability and pore size at maximum frequency of the supports on sintering temperature (1100−1175 °C).

mechanical strength or allow the particles to get in to the deep inside of pore.

To find the optimal sintering temperature, we measured the gas permeability and pore size of the supports as a function of sintering temperature. Figure 6 shows the pore size distribution determined by mercury porosimetry for the porous supports sintered at 1100−1175 °C. The distribution was in the rage of 1−3 μm, which is in agreement with that observed in the SEM images. For the support sintered at 1150 °C, the distribution was narrower than those of the others. Figure 7 shows the gas permeability and the pore size at maximum frequency as a function of sintering temperature from 1100 to 1175 °C. Expectedly, both gas permeability and pore size decreased with an increase in the sintering temperature. The maximum value of desired pore size for porous support is considered to be less than 2 μm because 1−3 μm sized particles is used for forming dense films. However, for the support sintered at 1100 °C, the pore size is rather larger than the maximum value. On the other hand, the gas permeability of the supports was high enough to transport oxygen to supported membranes at a sufficient rate, although the sintering at higher than 1150 °C significantly degraded the gas permeability because of the decrease in

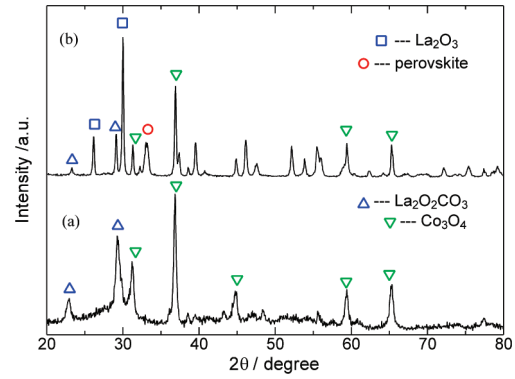

Figure 8. XRD patterns of powder after calcinations at (a) 400 and (b) 800 °C.

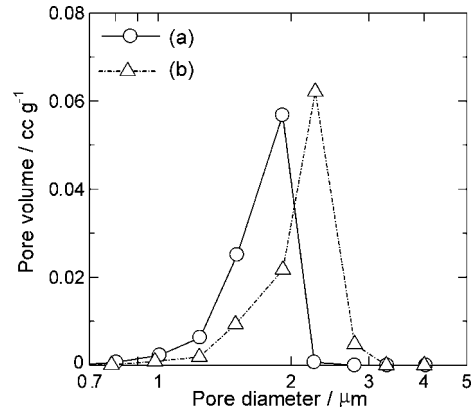

Figure 9. Pore size distribution of the porous supports using powder calcined at (a) 400 and (b) 800 °C.

the pore volume, as shown in Figure 6. Another requirement is that the supports should have a sufficient thermal resistance during the fabrication process of supported dense layers and oxygen permeation measurements. Thus, it is preferable that the supports are sintered at a temperature as high as possible prior to use. On the basis of the above considerations on the gas permeability and thermal stability, therefore, we selected 1150 °C as an optimal sintering temperature for the fabrication of the porous supports.

As mentioned above, we used metal oxalates to obtain irregular-shaped particles. However, such oxalates may generate CO_2 while calcinating, and then the generated gas may seem to make the pore structure because La oxycarbonate presented in the powder after calcination at 400 °C. To clear the influence of CO_2 generation on the pore formation, we investigated the relation between calcination temperature and pore structure. Figure 8 shows the XRD patterns of powder after calcination at 400 and 800 °C. It is found that powder calcined at 400 °C presented mainly La oxycarbonate and Co_3O_4, but that calcination at 800 °C gave La_2O_3. In other words, it is clear that the amount of La-oxycarbonate was decreased with increasing in the calcinations temperature. Figure 9 shows the pore size distribution determined by mercury porosimetry for the porous supports sintered at 1150 °C using powders calcined at 400 and 800 °C. Though the amount of La oxycarbonate in powder calcined at 800 °C was decreased, it is found that porous structure could be successfully formed. This result indicates that CO_2 generation by the decomposition of La oxycarbonate

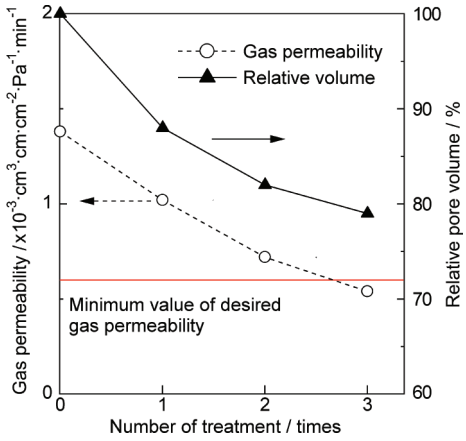

Figure 10. Dependence of the gas permeability and relative volume of the porous support on the number of heat-treatment cycles.

did not relate with the pore generation. Therefore, it seems that the low packing density using irregular-shaped particles was mainly reason for pore generation in this study.

To verify the feasibility of the fabricated supports, we investigated the thermal stability of the porosity in the supports at high temperature. For the stability test, the porous support sintered at 1150 °C was kept at 1050 °C for 5 h, and then the gas permeability was measured. For another stability test, the support was heat-treated at 1150 °C for 5 h, and it repeated three times. It was found that the gas permeability was not degraded and almost constant (1.3×10^{-3} cm^3 cm cm^{-2} Pa^{1-} min^{-1}) even after the treatment at 1050 °C (graph not shown), confirming that no significant change in the gas permeability of the support would occur during operation of oxygen separation at an elevated temperature such as 900 °C. Figure 10 shows the gas permeability and relative volume of pores in the support after the repeated heat-treatment at 1150 °C. The relative pore volume was defined as the total pore volume after the repeated treatment to that of a fresh support. The relative pore volume was roughly determined by measuring the volume of samples before and after treatment cycles. With an increase in the number of the treatment, the gas permeability and relative volume were decreased. After the third heat-treatment, the gas permeability became smaller than the desired value of 6.0×10^{-4} cm^3 cm cm^{-2} Pa^{1-} min^{-1}. However, the support exhibited sufficient gas permeability even after first and second heat-treatments. Thus, it is suggested that a supported membrane can be sintered and densified at 1150 °C without remarkable degradation of the porosity of the support.

Fabrication of a Dense Membrane on the Porous Support. To fabricate a dense membrane on the porous supports, precursor particles of LCC were prepared through an amorphous malic-acid precursor (AMP) method. Various dense membranes of substituted perovskite-type oxides with complex compositions have been fabricated by such complexation methods using citrate acid.[3,4,6,7,13,15,17] Here, we tried to form a dense thin LCC membrane on the porous supports by coating a slurry dispersing LCC particles and subsequent densification. Prior to the deposition, the precursor LCC particles were calcined at 900 °C for 5 h to obtain LCC particles for coating. The XRD pattern of the LCC

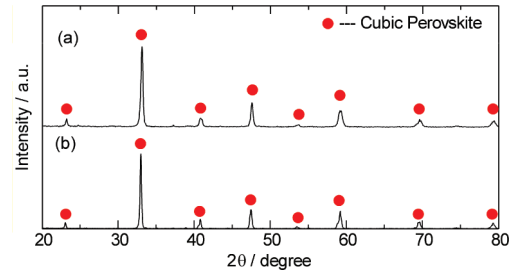

Figure 11. XRD patterns of (a) LCC ($La_{0.6}Ca_{0.4}CoO_3$) particles prepared through the AMP method at 900 °C and (b) the supported membrane fabricated at 1150 °C.

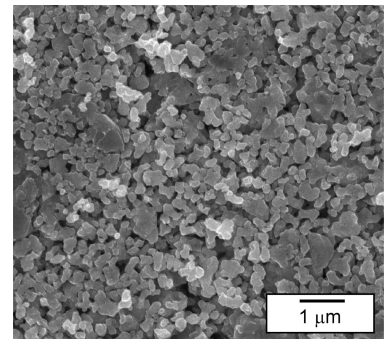

Figure 12. SEM photograph of the LCC ($La_{0.6}Ca_{0.4}CoO_3$) particles prepared through the AMP method at 900 °C.

particles thus prepared was shown in Figure 11a. The crystal phase can be ascribed to the cubic perovskite-type, which is consistent with that of the support shown in Figure 3b. This consistency in the composition between the support and the particles to be deposited is essential to fabricate a crack free membrane on the support by avoiding the mismatch of thermal expansion between the support and the membrane-.However there are some low angle shoulder at ca. 41 and 58°. Mastin et al. reported that the crystal structure of $La_{0.6}Ca_{0.4}CoO_3$ calcined at 900 °C showed mixed-phase of orthorhombic and rhombohedral perovskite.[44] These low angle shoulders observed at ca. 41 and 58° might be related the mixture phase.

Figure 12 shows the SEM image of the LCC particles calcined at 900 °C. The particles showed a spherical shape, in contrast to the irregular shape of the LCC particles prepared through the oxalate method.The particle size distribution of the LCC particles was measured from the SEM image, as shown in Figure 13. The particle size was in the range of 0.7 to 2 μm and the particle size at maximum frequency was 2 μm. The observed narrow size distribution is preferable for the fabrication of dense membranes because of intimate packing of the particles. In the same figure, the pore size distribution of the support sintered at 1150 °C was also shown. The pore size and the particle size distributions well-overlapped each other, suggesting that the LCC particles can be deposited on the support without filtration of the particles through pores in a large size.

On the basis of the above preliminary results, we fabricated asymmetric membranes by coating LCC slurries with different concentrations on the support sintered at 1150 °C. The

(44) Mastin, J.; Einarsrud, M.-A.; Grande, T. *Chem. Mater.* **2006**, *18*, 1680–1687.

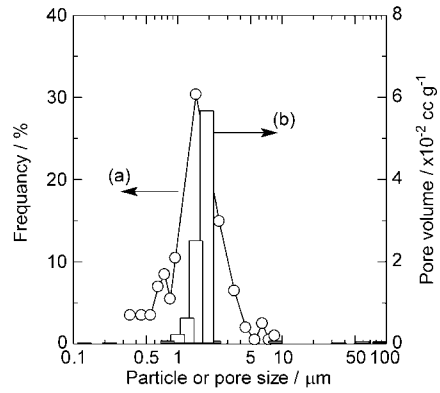

Figure 13. (a) Particle size distribution of the LCC ($La_{0.6}Ca_{0.4}CoO_3$) particles prepared through the AMP method at 900 °C and (b) pore size distribution of the porous support sintered at 1150 °C.

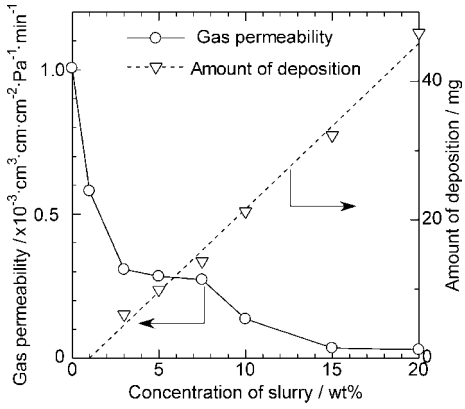

Figure 14. Gas permeability and the amount of deposited LCC particles on the supports as a function of slurry concentration for the asymmetric-structured membrane.

supported membrane fabricated using a 15 wt % slurry and by densification at 1150 °C was confirmed to have the cubic perovskite-type structure, as shown in Figure 11b. We next examined the effect of the concentration of slurries on the gas permeability of the fabricated asymmetric membranes, in order to optimize the fabrication conditions for gastight membranes. Figure 14 shows the amount of deposited particles which were determined by measuring sample weights before and after slurry coating, as a function of slurry concentration. The deposited amount monotonically increased with an increase in the slurry concentration. However, the amounts were about 25% lower than those calculated using the slurry concentrations and amounts of slurries used (0.3 mL). This means that some of particles whose sizes were far smaller than the pore size of the support were filtered through pores. Figure 14 also shows the gas permeability of the asymmetric membranes as a function of slurry concentration. The gas permeability decreased with increasing the slurry concentration, in conjunction with an increase in the amount of deposited particles. When the concentration of slurries was larger than 15 wt %, the gas permeability was almost negligible, reaching as low as 3.6×10^{-5} cm^3 cm cm^{-2} Pa^{1-} min^{-1} at 15 and 20 wt %. The observed trend was well-correlated with the surface morphology and the cross section of the supported membranes, as shown in Figure 13. At low concentrations (1 and 7.5 wt %), many pores were formed on the surface of the membranes (images a and

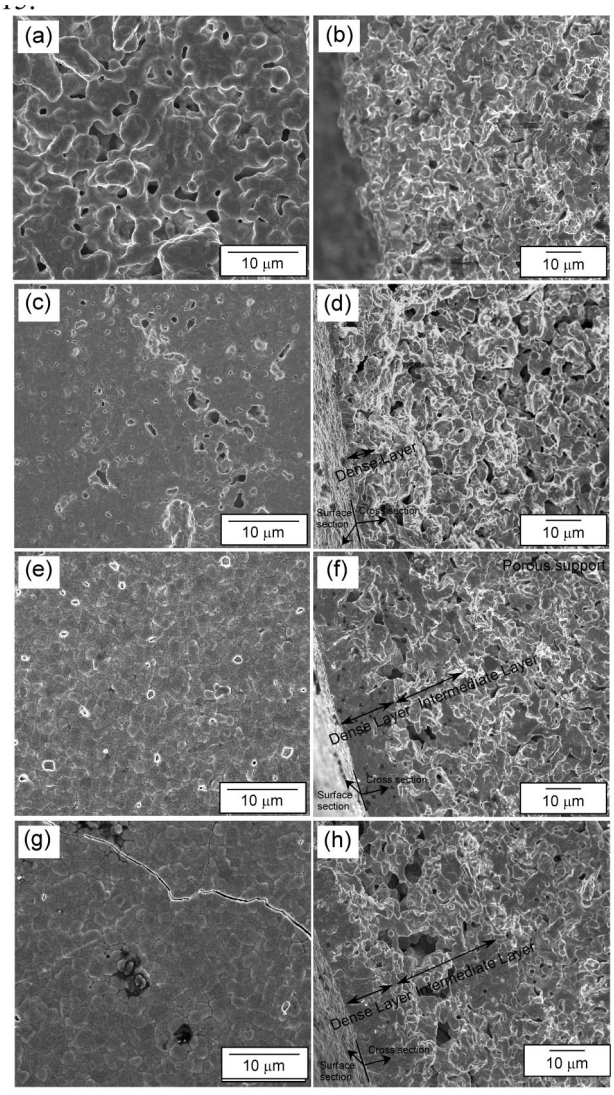

Figure 15. SEM photographs of the surface section of thin membranes fabricated using (a) 1, (c) 7.5, (e) 15, and (g) 20 wt % slurries, together with cross-sectional views of the asymmetric-structured membranes fabricated with (b) 1, (d) 7.5, (f) 15, and (h) 20 wt % slurries.

c in Figure 15). However, when the slurry concentration was increased to 15 and 20 wt %, no large pores could be seen (Figure 15e−h). On the other hand, for a 20 wt % slurry, clacks were formed on the surface, probably because of rapid drying of the slurry (Figure 15g). Thus, it can be concluded that the slurry concentration of 15 wt % is best-suited to fabricate crack-free dense membranes on the support.

It should be noted that, in the cross-sectional views shown in images f and h in Figure 15, another intermediate layer whose pore sizes are larger than those of the porous support can be seen between the dense layer and the porous support. To account for the mechanism of the formation of this layer, we observed the microstructure of the surface and the fractured cross-section of the asymmetric membrane fabricated using a 15% slurry without sintering, as shown in Figure 16 (high magnification image). The surface of the dense layer is quite flat and packed with particles of 200−300 nm with a narrow size distribution. On the other hand, however, large secondary particles of 1−10 μm and a lot of pores at the bottom of the dense layer were observed before sintering. This difference in morphology between the top and

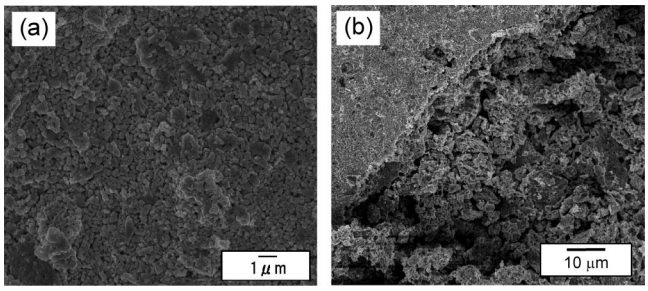

Figure 16. SEM photographs of (a) the surface and (b) fractured cross-section of the supported membrane (dense thin layer) fabricated using a 15 wt % slurry without sintering (dried at room temperature).

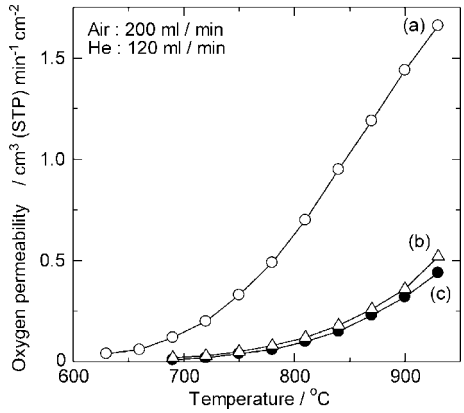

Figure 17. Oxygen permeabilities of (a) the asymmetric-structured membrane (10 μm) and disk-type membranes ((b) 580 and (c) 1200 μm).

the bottom of the dense layer may be due to a difference in the sedimentation rate between particles with different sizes. Of course, the used slurry solution included larger secondary particles than pore size because the concentration of slurry solution was dense. The sedimentation rate of such larger secondary particles is higher than that of smaller particles (primary and small secondary particles). Thus, it seems that slow sedimentation of smaller particles facilitated the formation of the dense layer packed with the particles at the top of the membrane, leading to the successful formation of the gastight membrane. On the other hand, it is considered that rapid sedimentation of large particles (secondary particles) formed the porous region at bottom of the dense layer, as shown in the SEM image. Preferably, the porous region may assist in the oxygen uptake by increasing the effective area of the membrane at the cathode side.

Oxygen Permeability of the Asymmetric Membrane. As revealed above, the careful control of the fabrication conditions successfully produced the thin gastight membrane (about 10 μm thickness) on the porous support. The thickness of the membrane was significantly reduced, as compared with the reported thicknesses (35−200 μm thickness) for other asymmetric membranes.[30−36] We next investigated the oxygen permeability as a function of temperature for the asymmetric membrane fabricated with a 15 wt % slurry and sintering at 1150 °C, as shown in Figure 17. The oxygen permeation flux was compared with typical disk-type membranes (580 and 1200 μm in thickness) fabricated with the LCC particles calcined at 900 °C. The disk membranes were sintered at 1150 °C for 5 h. For the asymmetric membrane, the oxygen permeation started at around 600 °C, and then

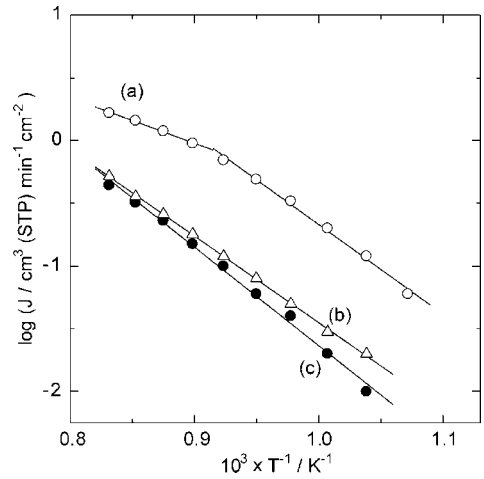

Figure 18. Arrenius plot of the oxygen permeation fluxes of (a) the asymmetric-structured membrane (10 μm) and disk-type membranes ((b) 580 and (c) 1200 μm).

abruptly increased with increasing temperature. The asymmetric membrane showed about four times higher oxygen permeability than the disk-type membrane at 930 °C, reaching a maximum permeation flux of 1.66 cm^3 (STP) min^{-1} cm^{-2}. For the disk-type membrane, the oxygen permeability slightly increased with decreasing in the thickness, for example 0.52 and 0.44 cm^3 (STP) min^{-1} cm^{-2}, respectively, for 580 and 1200 μm in thickness. However, the permeability observed in the asymmetric membrane, although it was so high, was lower than that expected from the Wagner equation (52.8 cm^3 (STP) min^{-1} cm^{-2}), which predicts that the oxygen permeation flux depends inversely on the thickness of the membrane, provided that the oxygen permeation is limited by the bulk diffusion of oxide ions as follows.

$$J_{O_2} = \{RT\sigma_e\sigma_i/[16F^2L(\sigma_e+\sigma_i)]\}\ln(P_{O_2,high}/P_{O_2,low})$$

where J_{O_2} is the oxygen permeation rate, L the membrane thickness, T the temperature, R the gas constant, F the Faraday constant, σ_e electronic conductivity, σ_i oxide ion conductivity, and $P_{O_2,high}$ and $P_{O_2,low}$ are oxygen partial pressures at the higher (oxygen feed side) and lower sides (sweep side), respectively. From these results, it follows that the oxygen permeation at 930 °C is likely controlled by not only bulk diffusion but also surface reaction for the present asymmetric membrane, as reported for other asymmetric membranes.[30−34,36] It is suggested that a slow surface reaction appears to be rate-determining for the membrane with the significantly reduced thickness.

Discussion on activation energy for the oxygen permeation process helps to better understand the permeation mechanism in the asymmetric membrane. Figure 18 shows the Arrehenius plot of the oxygen permeation flux for the estimation of the activation energy. As seen clearly in the figure, the relationship between logarithm of permeation flux and inversion of temperature yields straight lines. However, the slope of the straight line for the asymmetric membrane changed at 870 °C, whereas the slopes for the disk-type membranes were constant. The apparent activation energies in the lower and higher temperature ranges were calculated from the slopes to be 136.6 and 69.3 kJ mol^{-1}, respectively,

for the asymmetric membrane. The former value is similar to the activation energies of 132.0 kJ mol^{-1} and 139.6 kJ mol^{-1} calculated for 580 and 1200 μm thick of the disk-type membranes, respectively. From the above results, it is obvious that oxygen permeation for disk-type membranes based on LCC was controlled by bulk diffusion in the thickness of several 100 μm and more. Therefore, the activation energy for the asymmetric membrane was almost constant for the disk-type membranes with different thicknesses. It is reasonable to assume that the oxygen permeation for the asymmetric membrane is determined mainly by bulk diffusion at lower temperature below 870 °C. On the other hand, the activation energy at 870 °C and more decreased obviously from 136.6 to 69.3 kJ mol^{-1}. As discussed above, the oxygen permeation at 930 °C of the asymmetric membrane was suggested to be determined by both bulk diffusion and surface reaction. In addition, no phase transition around 800 °C was confirmed for $La_{0.6}Ca_{0.4}CoO_3$. Thus, it is considered that the observed change in the apparent activation energy is associated with a change in the rate-determining step from bulk diffusion to a mixed state of surface reaction and bulk diffusion. The calculated activation energy at the higher temperature region may not reflect a single step; it could include a mixed state of bulk diffusion and surface reaction. A similar temperature-dependence of the oxygen permeation flux was reported for a $Ba_{0.5}Sr_{0.5}Zn_{0.2}Fe_{0.8}O_3$ membrane by Wang et al., who attributed it to a change in the limiting step of the oxygen permeation process starting at a high temperature.[13] However, further work is necessary to elucidate the oxygen permeation mechanism for asymmetric membranes.

The obtained results demonstrate that the rate of oxygen permeation dramatically increased with decreasing the thickness of the membrane to approximately 10 μm. Moreover, a further increase in the oxygen permeability has been achieved using porous catalyst layers of $La_{0.6}Ca_{0.4}CoO_3$ or $SrCo_{0.8}Fe_{0.2}O_3$ attached onto the oxygen permeation side, as reported elsewhere.[40] Appropriate selection and design of the materials for the membrane as well as the catalyst layer would bring about a more substantial increase in the oxygen permeability.

Conclusions

The $La_{0.6}Ca_{0.4}CoO_3$ (LCC) porous support for asymmetric-structured membranes was fabricated by using irregular-shaped LCC particles prepared through the oxalate method. The optimization of the preparation conditions such as temperature, starting composition of metal ions, and oxalic acid concentration in a precursor solution, led to the formation of the supports with the desired composition. The precursor LCC particles with a low sinterability were useful to produce the LCC porous support with a mean pore diameter of 1.9 μm. As a result, the fabricated support exhibited high gas permeability of 1.4×10^{-3} cm^3 cm cm^{-2} Pa^{1-} min^{-1} and thermal stability even at high temperature of 1150 °C. Coating a 15 wt % slurry containing $La_{0.6}Ca_{0.4}CoO_3$ spherical particles, prepared through AMP method, on the support and subsequent calcination at 1150 °C successfully gave a thin gastight layer of 10 μm thickness. The oxygen permeability of the asymmetric membrane thus fabricated reached as high as 1.66 cm^3 (STP) min^{-1} cm^{-2} at 930 °C. The obtained results indicate that the present fabrication process for asymmetric membranes offers an efficient way to achieve high-performance oxygen separation from air. However, the observed value was lower than that expected from the Wagner equation, suggesting that the oxygen permeation in the asymmetric membrane is limited by both bulk diffusion and surface reaction. Nevertheless, it is possible to further increase the oxygen permeability by modification of the membrane surface with a porous catalytic layer and by an appropriate selection of base materials.

Acknowledgment. This work was partially supported by CREST of JST (Japan Science and Technology Corporation), Steel Industry Foundation for the Advancement of Environmental Protection Technology, and Hosokawa Powder Technology Foundation.

CM8013144